

Combined stellar structure and atmosphere models for massive stars

III. Spectral evolution and revised ionising fluxes of O3–B0 stars

Daniel Schaerer^{1,*} and Alex de Koter²

¹ Geneva Observatory, CH-1290 Sauverny, Switzerland

² NASA/GSFC, Advanced Computer Concepts, Code 681, Greenbelt, MD 20771

Received 17 May 1996 / Accepted 25 October 1996

Abstract. We provide an extensive set of theoretical spectral energy distributions of massive stars derived from our “combined stellar structure and atmosphere models”. The calculations cover the entire main sequence evolution for initial masses $M_i = 20 - 120 M_\odot$, corresponding to O3–B0 stars of all luminosity classes.

We predict detailed line blanketed UV spectra along the main sequence evolution. The major result is a systematic study of ionizing fluxes covering the entire parameter space of O and early B stars. We demonstrate the importance of accounting simultaneously for non–LTE effects, line blanketing and stellar winds to obtain an accurate description of the spectra of these stars shortward of the Lyman limit. The main results from our spectra are the following:

- ◊ The flux in the He II continuum is increased by 2 to 3 (3 to 6) orders of magnitudes compared to predictions from plane parallel non–LTE (LTE) model atmospheres. This reconfirms the work of Gabler et al. (1989).
- ◊ The flux in the He I continuum is known to be increased due non–LTE effects. However, we find that it is also influenced by wind effects as was previously found by Najarro et al. (1996) and Schaerer et al. (1996b). The combined effect of a mass outflow and line blanketing leads to a flatter energy distribution in the He I continuum, which confirms the results of Sellmaier et al. (1996) for a wider range of stellar parameters.
- ◊ The flux in the Lyman continuum is also modified due to line blanketing and the presence of a stellar winds,

although to a lesser degree than the spectrum at higher energies.

We derive revised ionizing fluxes for O3 to B0 stars based on the recent temperature and gravity calibrations of Vacca et al. (1996). The total number of Lyman continuum photons is found to be slightly lower than previous derivations. For most cases the differences are less than $\sim 20\%$. Due to the increased flux in the He I continuum the hardness ratio of the He I to H continuum is increased by ~ 1.6 to ~ 2.5 depending on spectral type and luminosity class.

In the view of recent EUV and X-ray observations, a critical discussion of current model assumptions (including our own) shows that for stars of spectral types later than approximately B0, which have relatively weak stellar winds, reliable predictions of ionizing fluxes are not yet possible. We identify the most likely physical reasons for this finding.

Key words: stars: atmospheres – stars: mass-loss – stars: early-type – ultraviolet: stars – H II regions

1. Introduction

The recent combined stellar structure and atmosphere (*CoStar*) models for massive stars of Schaerer et al. (1996a, b, hereafter Paper I and II) consistently treat the stellar interior, photosphere and wind using up-to-date input physics. An immediate advantage of this approach is that we predict the emergent spectral energy distribution along the evolutionary paths, which provides a large number of observable quantities ranging from the extreme ultraviolet (EUV) to the infrared (IR). Of particular interest is the spectral range shortward of the Lyman limit, where

Send offprint requests to: D. Schaerer

* Present address: Space Telescope Science Institute, 3700 San Martin Drive, Baltimore, MD 21218, USA (schaerer@stsci.edu)

the bulk of the bolometric luminosity of hot star is emitted. This wavelength range has been recently observed in early-type stars by Hoare et al. (1993) and Cassinelli et al. (1995, 1996).

From both theoretical and observational results, it has become clear that the flux shortward of the Lyman edge is not only affected by line blanketing and non-LTE effects but is also influenced by the presence of a stellar wind. The presence of a stellar wind may considerably change the formation of the flux in the Lyman continuum up to high frequencies. This was first pointed out by Gabler et al. (1989), who showed that a wind can cause a significant depopulation of the He II ground state. As a consequence, models accounting for stellar winds lead to He⁺ ionizing fluxes which are ~ 2 –3 orders of magnitudes larger than the values predicted from non-LTE plane parallel models (see Gabler et al. 1992, Paper II). With respect to the widely used LTE models of Kurucz (1991) the increase is 3–6 orders of magnitude! More recently evidence has been presented that the flux at longer wavelengths, i.e. in the He^o continuum (at $\lambda < 504$ Å) and even in the Lyman continuum (at $\lambda < 912$ Å), can also be affected by the presence of a stellar wind (Paper II, Najarro et al. 1996). As in the case of the He⁺ ionizing flux this occurs through a depopulation of the corresponding ground states.

The above illustrates the importance of treating the stellar wind when predicting ionizing fluxes. The first results of these theoretical studies have already had important consequences for the interpretation of observations:

- The strong increase of He⁺ ionizing photons in the models of Gabler et al. (1991) leads to an important reduction of the Zanstra–discrepancy in central stars of planetary nebulae.
- Nebular calculations using emergent fluxes from wind models yields an improved match to the observed ionization structure of H II regions, thereby resolving the so-called [Ne III] problem (Sellmaier et al. 1996, Rubin et al. 1995 and references therein).
- EUVE observations of the Lyman continuum flux of the B2II giant ϵ CMa by Cassinelli et al. (1995) have provided a first *direct comparison* with model atmospheres. Surprisingly the observations show a flux significantly larger than predicted from both LTE and non-LTE plane parallel models. Among several alternative explanations for this failure of plane parallel atmosphere models (Hubeny & Lanz 1996), Najarro et al. (1996) suggest that the discrepancy of the Lyman continuum flux may be reduced if one accounts for the weak stellar wind of ϵ CMa.

The above findings clearly point out the necessity to improve our understanding of the ionizing fluxes of OB-type stars. While the first studies have concentrated on individual objects and very few models are available yet, our study covers the entire main sequence evolution between 20 and 120 M_{\odot} , i.e. spectral types O3 to early-B,

and provides predictions from elaborate non-LTE calculations including line blanketing and stellar winds. This will allow to work out the consequences of revised ionizing fluxes for a large number of systems, including the galactic ISM, H II regions and starbursts. Such direct or indirect comparisons with observations will, in turn, be of great value for testing our predictions and improve the reliability of model atmospheres for hot stars.

The remainder of the paper is structured as follows: Our method and the calculated model set are described in Sect. 2. Predicted UV line blanketed spectra are presented in Sect. 3. The main presentation and discussion of the ionizing fluxes takes up Sect. 4. Section 5 contains our revised calibration of ionizing fluxes and contains comparisons to previous work. In Sect. 6 we discuss uncertainties of the present models and point out future improvements. The main results are summarised in Sect. 7.

2. Model calculations

2.1. Input physics and method

A detailed description of our so-called *CoStar* models and the input physics adopted for the calculations is given in Paper I of this series. Here, we will only briefly summarise the most important characteristics of our models.

The entire star, comprising the stellar interior and a spherically expanding atmosphere including the stellar wind, is treated consistently. The interior is modelled with the Geneva stellar evolution code using the same input physics (reaction rates, opacities etc.) as in the latest grid calculations of Meynet et al. (1994). The atmosphere is modelled using the ISA-WIND code of de Koter et al. (1993, 1996b). Outer boundary conditions for the stellar interior calculations are given by the atmospheric structure. Basically the atmosphere is characterised by two parts: the subsonic regime with an extended photosphere and the wind, where the flow is accelerated to the terminal flow velocity v_{∞} . For the photospheric part we solve the stationary momentum equation taking into account gas and radiation pressure. The subsonic part is smoothly connected with a wind structure described by the usual “ β -law” (see Paper I). The temperature structure is given by radiative equilibrium in an extended grey atmosphere following Lucy (1971) and Wessolowski et al. (1988). In the final step, a consistent solution is constructed, embracing both the stellar interior and the atmosphere. In addition to the usual predictions from evolutionary models, *CoStar* models also provide the detailed emergent fluxes along the evolutionary paths.

The adopted mass loss rate and the additional parameters required to describe the wind structure are taken as in Paper I:

- Mass loss rates are adopted as in Meynet et al. (1994). This means that for population I stars throughout the HR diagram we use the mass loss rates given by de

Jager et al. (1988), enhanced by a factor of two. Justifications for this choice are given by Meynet et al. (1994) and Maeder & Meynet (1994). For non-solar metallicities \dot{M} was scaled with $(Z/Z_{\odot})^{\zeta}$, where $Z_{\odot} = 0.020$. Consistent with our previous grid calculations an exponent $\zeta = 0.5$ was taken as indicated by wind models (Kudritzki et al. 1987, 1991).

- The terminal velocities v_{∞} as a function of metallicity are from wind models of Leitherer et al. (1992). Comparisons of our adopted terminal velocities with observations of population I stars have been discussed in Paper I.
- For the rate of acceleration of the supersonic flow we take $\beta = 0.8$ following theoretical predictions of Friend & Abbott (1986) and Pauldrach et al. (1986). These predictions are in good agreement with observations of O stars by Groenewegen & Lamers (1991).

The ISA-WIND non-LTE radiation transfer calculations, which yield the detailed spectral evolution use the atmospheric structure from the *CoStar* model summarised above. In ISA-WIND, the line transfer problem is treated using the Sobolev approximation, including the effects of the diffuse radiation field, and the continuous opacity inside the line resonance zone (de Koter 1993, de Koter et al. 1993). Line blanketing is included following the opacity sampling technique introduced by Schmutz (1991). The method involves a Monte Carlo radiation transfer calculation including the most important spectral lines of all elements up to zinc. We want to make clear that our models are not fully “line blanketed” in the context established in photospheric models, i.e. a fully consistent treatment of the effects of the presence of lines on the atmospheric structure and emergent spectrum. However, we opted to use this term rather than the term “line blocked” because the latter would go by the fact that we *do* treat the redistribution of flux and – although in an approximate way – the effect of blocking on the temperature structure. The ionization and excitation of the metals is treated as in Schaerer & Schmutz (1994a,b) to which the reader is referred for a detailed description of the entire procedure.

The input physics for the atmospheric structure calculations consists of atomic data for the elements explicitly included in the non-LTE model. In the present work hydrogen and helium are treated as summarised in Paper I. The H, He, C, N, and O composition of the atmosphere is that corresponding to the outermost layer of the interior model. For the metals included in the line blanketed atmosphere, the abundances of Anders & Grevesse (1989) have been adopted.

The domain where our models are applicable is limited to relatively strong winds because of several simplifying assumptions made in the calculations (see also Sect. 6 for a critical discussion):

- ◊ The Sobolev approximation yields good agreement with comoving frame calculations for O and WR stars

(de Koter et al. 1993). However, for weaker winds differences in the level populations will progressively affect the predicted continuum fluxes in particular shortward of the Lyman edge.

- ◊ Presently our calculations neglect line broadening, yielding only a poor treatment of photospheric lines. This results in an underestimate of blanketing in the photosphere. For the early spectral types and/or strong winds this approximation should not be crucial, since in these cases photospheric lines are both weaker and less numerous, and wind effects play a very important role in establishing the equilibrium population.
- ◊ The temperature structure, which is derived from radiative equilibrium in an extended grey atmosphere, includes line blanketing only in an approximate way. Even with the improved treatment of Schaerer & Schmutz (1994a), the determination of the temperature structure in the photosphere-wind transition zone remains somewhat uncertain. In the case that wind effects dominate, this effect should not be of importance.
- ◊ We neglect X-rays which, for stars with relatively weak winds, can drastically alter the ionization structure (MacFarlane et al. 1994) and might also provide an additional heating mechanism.

Despite these uncertainties, we will argue below that the O stars covered in the present paper should be quite adequately treated with our techniques. However, we do note that because of the above mentioned points and because of other indications (see Sects. 6.1,6), for B stars reliable predictions of the ionizing fluxes are not yet possible. Future improvements will be necessary to extend the range of validity of the models.

2.2. Selected models

To provide a complete coverage of the entire main sequence (MS) evolution with our *CoStar* models we have calculated evolutionary tracks for initial masses of 20, 25, 40, 60, 85 and 120 M_{\odot} at solar metallicity. This paper includes the results from Papers I and II, which covered the range from 40 to 85 M_{\odot} . Additionally, we provide calculations for the entire data set at low metallicities ($Z=0.004$). A high metallicity grid is in preparation. The continuum spectral energy distributions from both the $Z=0.020$ and 0.004 model sets are available on request from the authors. They will also be included in a recent CD-ROM distributed by the AAS (Leitherer et al. 1996).

2.2.1. Solar metallicity: $Z=0.020$

Figure 1 shows the evolutionary tracks at $Z=0.020$ in the HR-diagram and the $\log g - \log T_{\text{eff}}$ diagram. For each track, we have selected several models for which the stellar parameters are summarized in Table 1. Along each MS track the models have been selected according to the following criteria if possible : 1) ZAMS model, 2)-5) $\log g$

Table 1. Summary of selected models at $Z=0.020$: stellar parameters and approximate spectral classification

model #	age [yr]	$\frac{M}{M_{\odot}}$	$\log T_{\text{eff}}$ [K]	$\log \frac{L}{L_{\odot}}$	$\log g$ [cm s $^{-2}$]	$\frac{R_{*}}{R_{\odot}}$	$\log \dot{M}$ [$M_{\odot}\text{yr}^{-1}$]	v_{∞} [km s $^{-1}$]	n_{H}	μ	SpType ($T_{\text{eff}}-M_{\text{bol}}$)	SpType (HRD)
20 M_{\odot} track:												
A1	$4.00 \cdot 10^4$	20.00	4.551	4.658	4.24	5.633	-7.058	2890.	0.90	0.634	O8V	B0V
A2	$3.65 \cdot 10^6$	19.60	4.523	4.767	4.01	7.268	-6.857	2544.	0.90	0.634	O9V	B0V
A3	$6.15 \cdot 10^6$	19.15	4.483	4.872	3.73	9.860	-6.634	2202.	0.90	0.634	B0V	B0IV
A4	$7.79 \cdot 10^6$	18.65	4.401	4.966	3.30	16.034	-6.384	1802.	0.90	0.634	B0.5II	B0.5II
25 M_{\odot} track:												
B1	$2.75 \cdot 10^4$	25.00	4.586	4.907	4.22	6.387	-6.806	2897.	0.90	0.634	O7V	O9.5V
B2	$2.60 \cdot 10^6$	24.48	4.560	4.997	4.02	7.994	-6.596	2589.	0.90	0.634	O8V	O9V
B3	$4.79 \cdot 10^6$	23.71	4.514	5.103	3.71	11.187	-6.307	2208.	0.90	0.634	O9IV	O8.5V
B4	$5.89 \cdot 10^6$	22.99	4.443	5.171	3.35	16.710	-6.066	1868.	0.90	0.634	B0II	O9.5III
40 M_{\odot} track:												
C1	$4.04 \cdot 10^4$	39.98	4.646	5.376	4.20	8.326	-6.463	2962.	0.90	0.634	O5V	O7V
C2	$1.50 \cdot 10^6$	39.25	4.621	5.447	4.02	10.152	-6.170	2690.	0.90	0.634	O6V	O7V
C3	$2.85 \cdot 10^6$	37.86	4.577	5.519	3.76	13.457	-5.809	2354.	0.90	0.634	O7IV	O7IV
C4	$3.81 \cdot 10^6$	35.48	4.481	5.578	3.29	22.422	-5.414	1893.	0.90	0.634	O9.5II	O9.5I
C5	$4.08 \cdot 10^6$	34.35	4.414	5.597	2.98	31.215	-5.290	1660.	0.90	0.634	B0I	O9.5I
C6	$4.38 \cdot 10^6$	32.38	4.268	5.628	2.34	63.521	-5.126	1269.	0.90	0.634	B2I	O9.5I
60 M_{\odot} track:												
D1	$8.72 \cdot 10^4$	59.96	4.681	5.731	4.16	10.663	-6.090	3050.	0.90	0.634	O4V	O5.5V
D2	$7.72 \cdot 10^5$	59.20	4.664	5.766	4.05	12.010	-5.856	2883.	0.90	0.634	O4.5V	O5.5V
D3	$2.23 \cdot 10^6$	55.03	4.597	5.842	3.68	17.838	-5.252	2381.	0.90	0.634	O6III	O5.5IV
D4	$2.76 \cdot 10^6$	50.60	4.508	5.867	3.26	27.672	-4.931	1960.	0.90	0.634	O9 I	O7I
D5	$3.00 \cdot 10^6$	47.43	4.420	5.879	2.86	42.147	-4.826	1646.	0.90	0.634	B0I	O7I
D6	$3.23 \cdot 10^6$	43.68	4.344	5.897	2.50	60.890	-4.779	1391.	0.87	0.666	B0.5I	O7.5I
D7	$3.44 \cdot 10^6$	40.01	4.352	5.920	2.48	60.392	-4.747	1319.	0.80	0.737	B0.5I	O7I
85 M_{\odot} track:												
E1	$5.00 \cdot 10^4$	84.88	4.708	6.004	4.14	12.900	-5.683	3182.	0.90	0.634	O3IV	O4V
E2	$7.10 \cdot 10^5$	82.84	4.686	6.034	4.01	14.780	-5.379	2977.	0.90	0.634	O3.5IV	O4.5IV
E3	$1.66 \cdot 10^6$	75.58	4.629	6.071	3.71	20.017	-4.879	2538.	0.90	0.634	O5III	O4.5III
120 M_{\odot} track:												
F1	$4.18 \cdot 10^4$	119.54	4.728	6.248	4.13	15.603	-5.147	3340.	0.90	0.634	O3V	O3IV
F2	$6.26 \cdot 10^5$	116.48	4.702	6.275	4.00	17.789	-4.853	3103.	0.90	0.634	O3III	O3.5III
F3	$2.12 \cdot 10^6$	80.43	4.675	6.282	3.71	20.681	-4.572	2428.	0.75	0.795	O3I	O3.5I

approximately 4., 3.7, 3.3, 3., and 6) maximum radius. One additional TAMS model is available for the 60 M_{\odot} track. The total of 27 models should provide a good coverage of the entire MS spectral evolution.

The following entries are given in Table 1: Model number (column 1), age (2), present mass (3), effective temperature (4), luminosity (5), gravity (6), stellar radius (7), mass loss rate (8), terminal velocity (9), number fraction of hydrogen n_{H} normalised to $n_{\text{H}} + n_{\text{He}} = 1$. (10) and the mean molecular weight per free particle μ (11) used to determine the photospheric structure. The last two columns give an approximate spectral classification, which has been obtained from a nearest neighbour search in the tables

of Schmidt-Kaler (1982)¹ The assignment in column 12 uses the variables $(T_{\text{eff}}, M_{\text{bol}})$ ², while a nearest neighbour search in the HR-diagram yields the spectral types in column 13.

2.2.2. Low metallicity calculations: $Z=0.004$

For the low metallicity models, we have chosen the following approach: instead of calculating full *CoStar* models we have calculated atmosphere models at the same position

¹ At this point, we adopt the Schmidt-Kaler classification instead of the more recent one from Vacca et al. (1996) since the latter does not cover the entire domain of our models.

² We specify T_{eff} in kK, which gives a reasonably large weight to the temperature.

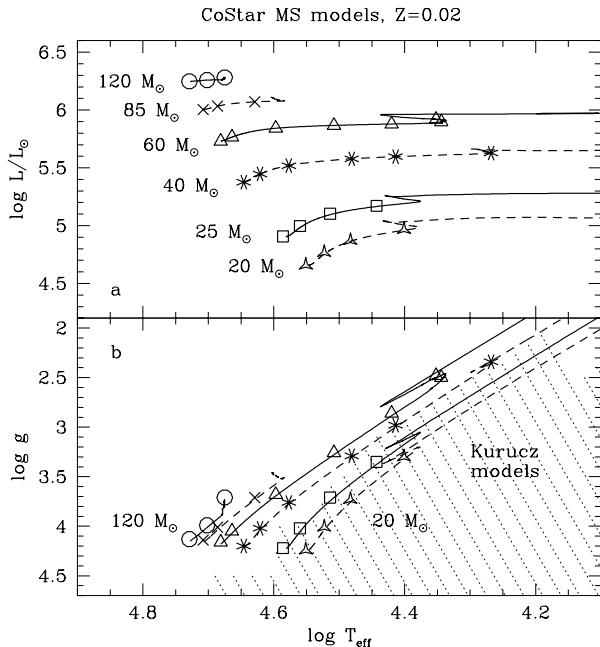


Fig. 1. **a** HR-diagram covering the MS phases for all initial masses. The WR stage during the H-burning phase of the 85 and 120 M_{\odot} models are not included. Symbols (circles, crosses etc.) denote the selected models describing the spectral evolution (see Table 1). **b** $\log g - \log T_{\text{eff}}$ diagram corresponding to **a**. The hatched area shows the domain for which Kurucz atmosphere models are available

in HR-diagram, i.e. adopting identical stellar parameters as for $Z=0.020$. Only the wind parameters (\dot{M} , v_{∞}) and the composition have been adapted to $Z=0.004$. This procedure allows detailed comparisons between the emergent spectra at different metallicities.

The following changes apply for $Z=0.004$ with respect to the parameters given for $Z=0.020$ in Table 1: \dot{M} is reduced by a factor of 2.236, and v_{∞} is reduced by 1.233 to reflect the dependence expected from wind models (cf. Sect. 2.1). In addition to accounting for the abundance changes of metals, one also needs to modify the relative hydrogen to helium abundance. Consistently with recent evolutionary grid calculations (Charbonnel et al. 1993, Meynet et al. 1994), we adopt an initial helium content, $Y = Y_p + (\Delta Y/\Delta Z) Z$ with a $\Delta Y/\Delta Z$ ratio of 3. (see Schaller et al. 1992). The resulting abundances for $Z=0.004$ are: $(X, Y) = (0.744, 0.252)$ in mass fraction, which corresponds to H and He number abundances of $(n_{\text{H}}, n_{\text{He}}) = (0.922, 0.078)$. These abundances apply to all $Z=0.004$ models since, in contrast to the solar metallicity tracks, no surface He enrichment is expected in this case (see Meynet et al. 1994). Consequently the mean molecular weight μ , which enters in the determination of the atmospheric structure in the low velocity domain is given by $\mu = 0.600$.

For solar metallicity we will discuss several results in detail. For the reduced metallicity, we will present the integrated ionizing fluxes at $Z=0.004$ and briefly summarise the influence of metallicity on the emergent spectra.

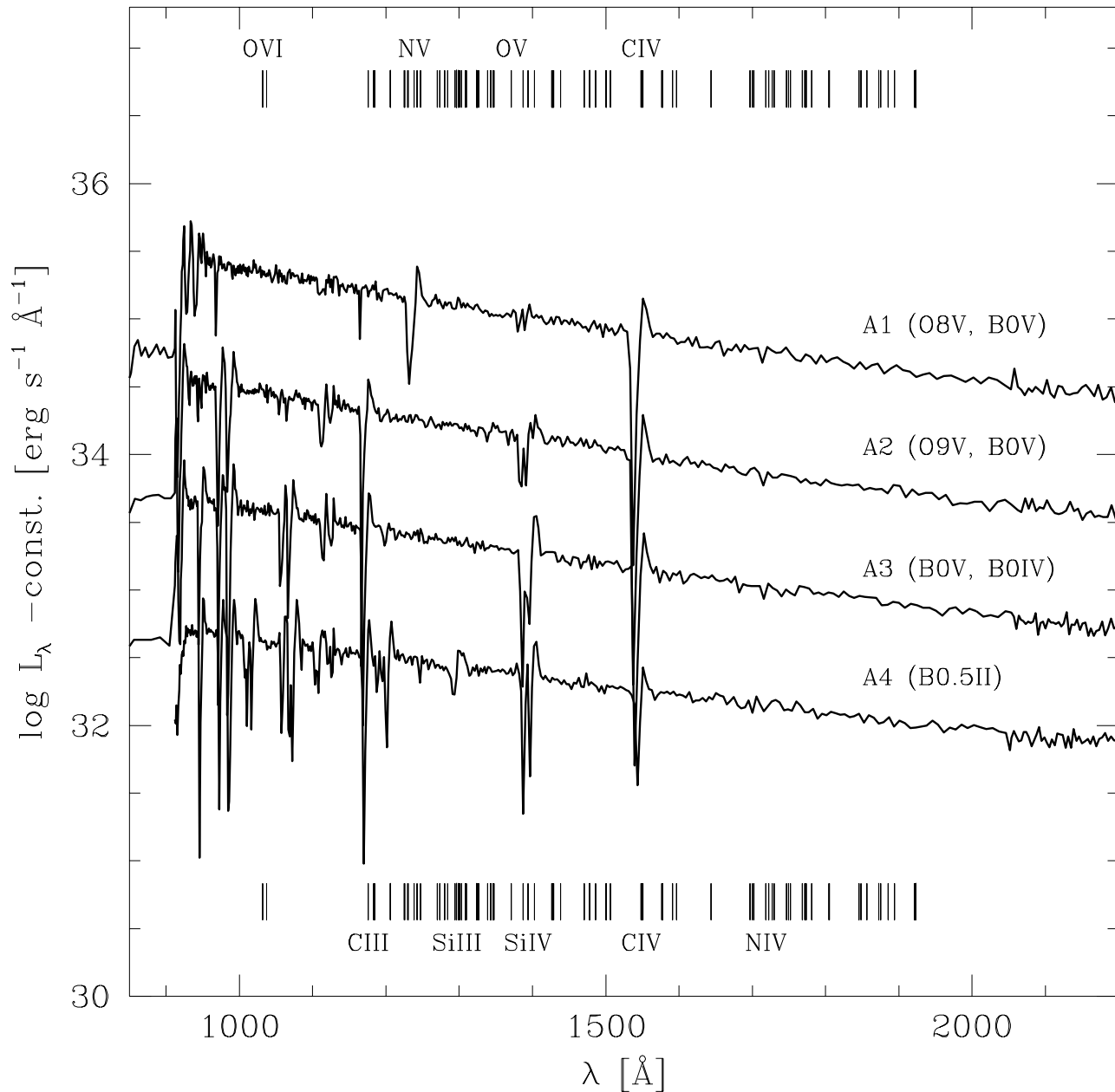
CoStar: $20 M_{\odot}$, $Z=0.02$, main sequence

Fig. 2. Synthetic UV spectra showing the spectral evolution on the $20 M_{\odot}$ track. Plotted is the logarithm of the emergent luminosity. Approximate spectral types from Table 1 are given. Starting with the second model, each spectrum has been shifted downwards by 0.7 dex with respect to the previous one, in order to allow a good comparison. The marks on the top and bottom indicate the location of the CNO and Si lines taken from the lists of Bruhweiler et al. (1981) and Dean & Bruhweiler (1985). The strongest CNO, and Si features are labeled

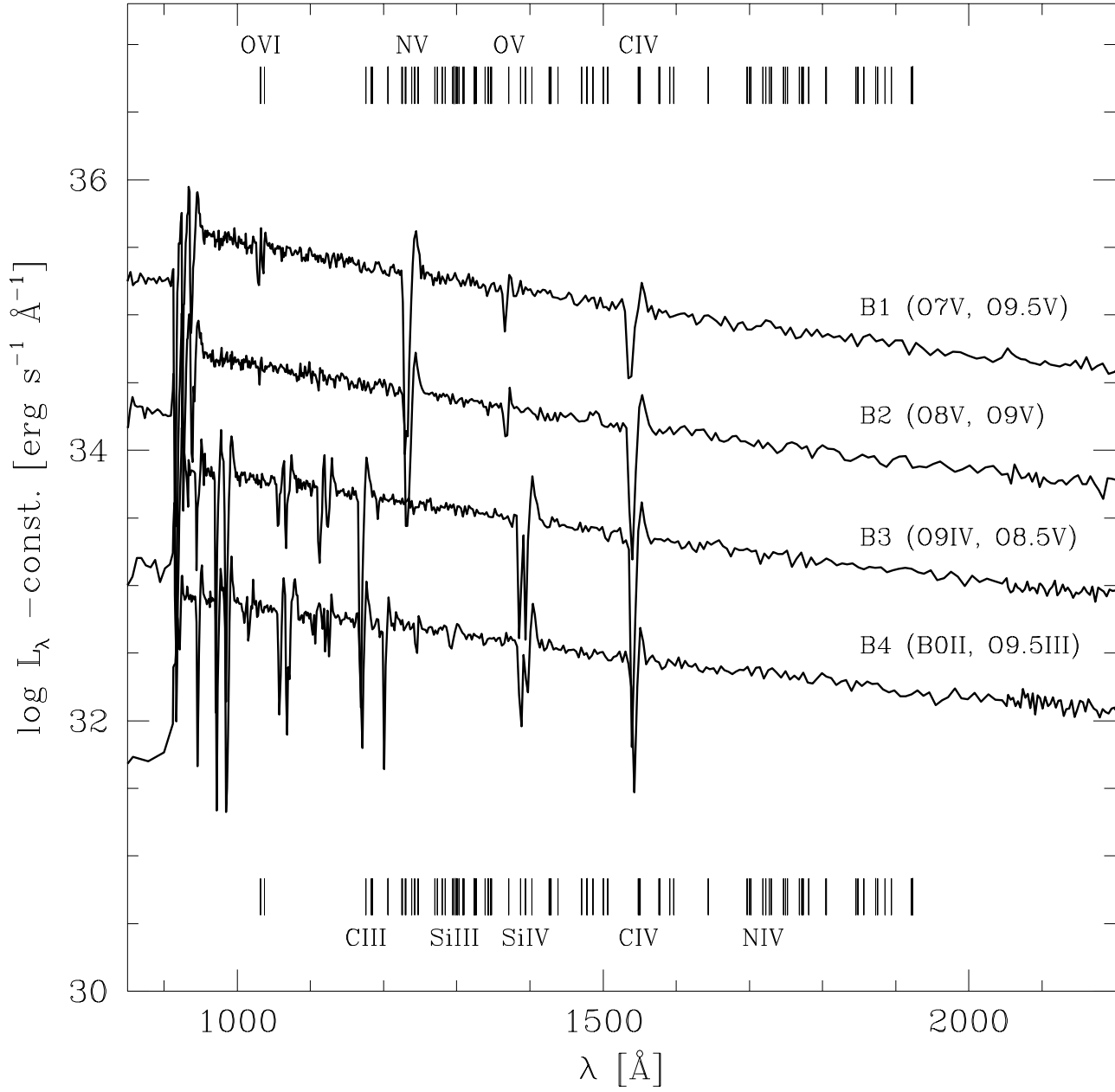
CoStar: $25 M_{\odot}$, $Z=0.02$, main sequence

Fig. 3. Same as Fig. 2 for the $25 M_{\odot}$ track (models B1 to B4)

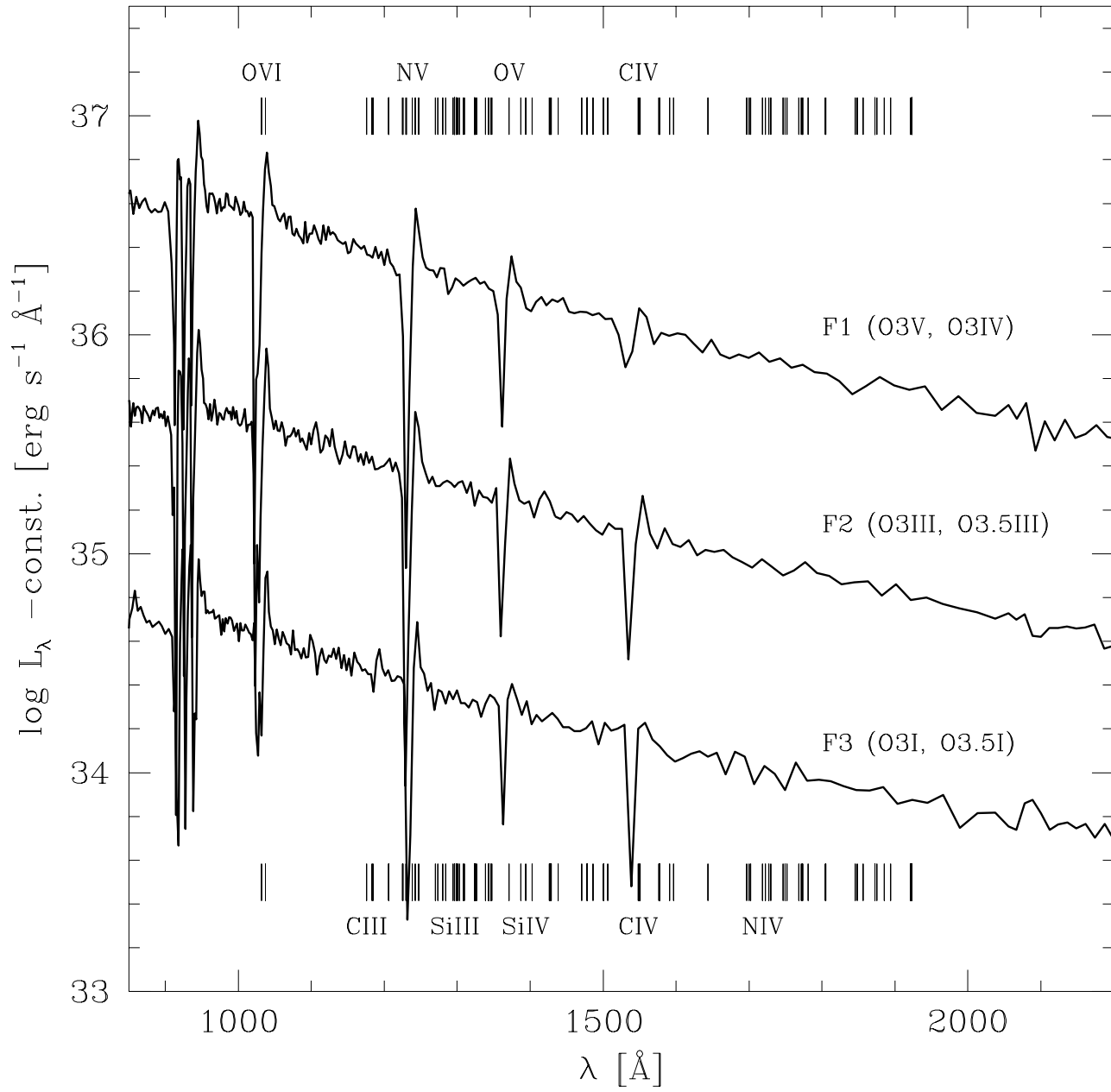
CoStar: 120 M_{\odot} , $Z=0.02$, main sequence

Fig. 4. Same as Fig. 2 for the 120 M_{\odot} track (models F1 to F3)

3. Evolution of the UV line blanketed spectrum at $Z=0.020$

Our line blanketed models allow us to predict a large number of detailed observable line features, which are well suited for comparison with UV spectra. In Paper II we have presented the spectral evolution in the 850 to 2200 Å range along MS tracks with initial masses between 40 and 85 M_{\odot} . To provide the complete set of UV spectra at solar metallicity we here present the corresponding results for the additional tracks ($M_i = 20, 25$ and $120 M_{\odot}$).

The synthetic UV spectra of the models given in Table 1 are plotted in Figs. 2 to 4. Together with the plots from Paper II, these figures illustrate the behaviour of the strongest UV features as a function of luminosity and effective temperature. The progressive behaviour of the strongest wind lines of CNO and Si agrees with the conclusions drawn in Paper II, where we refer to for more details.

(a) The predictions for the N v resonance line follows the observed decrease in line strength towards later spectral types. The spectra of the B-type stars show some tendency to produce less N v than observed, which reflects the problem of super-ionization.

(b) The strong luminosity dependence of the Si IV line is reproduced.

(c) While the C IV λ 1550 doublet is predicted too weak for ZAMS models with $M_i \gtrsim 40 M_{\odot}$, we obtain a strong C IV P-Cygni line for less massive ZAMS stars. Compared to observations (see Snow et al. 1994) the C IV line of the 20 and 25 M_{\odot} ZAMS models is too strong. Both results indicate that the predicted carbon ionization balance is shifted towards too high ionization stages for a given temperature (see Paper II).

(d) The predicted O v λ 1371 line shows a strong P-Cygni profile for the hottest models, while it is mostly observed in absorption. The reasons have been discussed in Paper II.

In Paper II we have performed several *quantitative* comparisons of metal line features. In particular we have been able to reproduce the strong observed Fe 1920 Å feature in late O and early-B giants and supergiants. This feature was found to be a good temperature indicator for these stars. The new tracks confirm this result.

4. Ionizing spectrum

In this section, we will compare our model predictions, which take into account non-LTE effects, line blanketing and a stellar wind, with both LTE and non-LTE plane parallel atmospheres. In this way, we can investigate the effect of a stellar wind on the emerging EUV continuum flux. Before doing so, we first briefly discuss the physics of the processes connected with the presence of a stellar wind that are found to affect the flux distribution shortwards of the Lyman continuum edge. There are three categories

of effects, wind velocity effects, geometrical wind effects, and line blanketing effects.

Wind velocity effects: Because of the velocity gradient in a stellar wind, the He II (I) groundstate may become depopulated. If this occurs in the region where the corresponding continuum is formed, this will lead to a decrease of the bound-free opacity and consequently to an increase of the flux at $\lambda < 228$ (504) Å.

The depopulation effect works as follows. We consider a point r in the wind, hereafter the local point. The velocity gradient in the wind flow allows helium resonance line photons to escape from r to infinity, forcing this transition out of detailed balance. The $n = 1$ level population is no longer controlled by the local contribution to the mean intensity in the line, \bar{J} , i.e. by the local line source function. Instead, \bar{J} is dominated by the non-local contribution which is proportional to the specific intensity at the photosphere. Because the radiation temperature at the photosphere is higher than the electron temperature $T(r)$ and because the helium resonance transition is in the Wien part of the spectrum, this will lead to a large increase of radiation at the line frequency, depopulating the groundlevel (see Gabler et al. 1989).

At a certain point in the wind, the depopulation reaches a minimum. Farther out, the $n = 1$ population will again increase because of the proportionality of \bar{J} to the dilution factor and because of an increased importance of recombinations from higher levels (see Najarro et al. 1996). We need to distinguish four cases:

(a-i) The continuum is formed in the region below (i.e. at higher Rosseland optical depth) that of the regime of strong depopulation of the groundstate. This would correspond to stars with low density winds. If the mass loss is so small that the continuum is formed in the photosphere, it will be likely that no significant changes from plane parallel models have occurred, consequently, the continuum flux will not differ much from a model without a stellar wind.

(a-ii) As in the first case, the mass loss is sufficiently low that the groundlevel does not suffer from the depopulation effect described above. What defines this case is that transitions between high lying levels become optically thin. Subsequent electron cascading causes the ground state population to increase. Consequently, the continuum flux will decrease somewhat relative to a model without a stellar wind. This case occurs in the He I continuum of most of the models considered in this work. In particular, the described effect causes a *flattening* of the spectrum in the He I continuum, since the continuum at relatively short wavelengths is formed at relatively large Rosseland optical depth, where it is less sensitive to the described effect.

(a-iii) The continuum is formed in the geometrical region corresponding to that of strong depopulation. The continuum flux will be increased significantly relative to a model without a stellar wind.

(*a-iv*) The continuum is formed in the region outside of that of the depopulation regime. This would correspond to models with a very dense wind. An increased flux relative to a model without a stellar wind may still be present, but the flux will not be as high as in the preceding case.

Case (*a-ii*) typically occurs in the He I continuum of most O-type models (cf. also Sellmaier et al. 1996). Case (*a-iii*) dominates the He II continuum of O-type stars. It may, however, also occur in the He I continuum of B-type stars (Najarro et al. 1996).

Geometrical wind effects: (*b*) Related to the above effects is the possibility that continuum forming layers may be located outside of the photosphere. In this case the flux is determined by the competing effects of (*b-i*) the increase of the emitting surface yielding a larger flux, and (*b-ii*) a drop in the local source function, at the emitting surface, due to the temperature decrease, which reduces the emergent flux. The geometrical effects mainly occur in the He II continuum, where the opacity is the largest.

Line blanketing effects: Line blanketing may either cause an increase or a decrease of the flux, because two competing effects play a role:

(*c-i*) The presence of many lines in the photosphere causes a redistribution of photons from the radiation field at $\lambda < 228$ (504) Å towards photons of longer wavelength. This blocking of photospheric flux causes a decrease in the helium ionization, increasing the He II (1) groundlevel population. Both the photospheric blocking and the increased He II (1) groundstate population cause a decrease of the flux at $\lambda < 228$ (504) Å.

(*c-ii*) As first shown by Schaerer & Schmutz (1994a), the presence of many resonance lines in the stellar wind causes an increase of the isotropy of the radiation field. This diffuse radiation is essentially the result of (multiple) photon scattering and occurs most effectively in wavelength regions where the line density is so large that the lines overlap. In these regions the star effectively shows a larger geometrical dilution factor compared to the case of no line blanketing. The associated increase in mean intensity yields a higher ionization, consequently a decrease in the groundstate population of He II (1) which causes an increase of the flux at $\lambda < 228$ (504) Å.

The first effect is usually more important in H I and He I continua and also dominates in the He II continuum of stars with low density winds. The last effect dominates in the He II continuum of stars with high density winds.

4.1. Comparisons of CoStar and plane parallel models

We first compare the EUV spectral range of *CoStar* models with plane parallel models. We limit our comparisons to models which include line blanketing. For the plane parallel models we adopt the widely used LTE models of Kurucz (1991, ATLAS9) and the recent non-LTE models from Kunze (1994, cf. Kunze et al. 1992). The latter provide an extensive grid, covering essentially the same

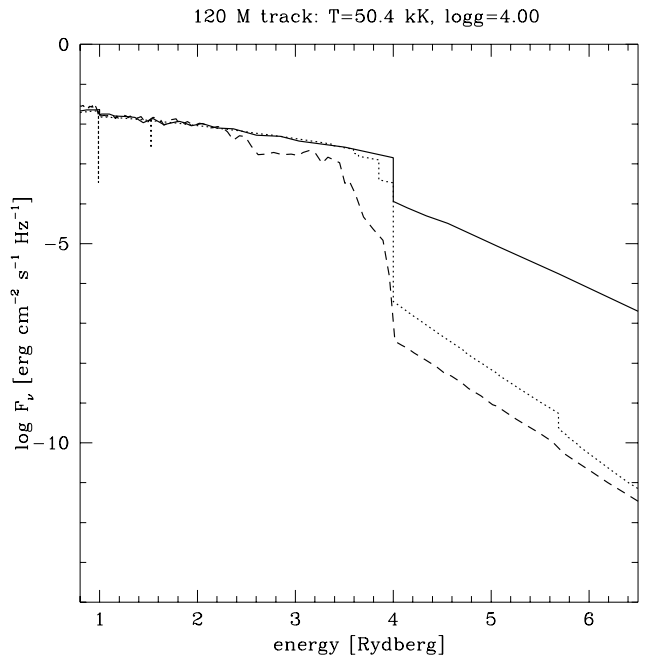


Fig. 5. Comparison of emergent EUV fluxes from a *CoStar* model (solid line), a plane parallel non-LTE model of Kunze (1994, dotted line) and a plane parallel LTE model of Kurucz (1991, dashed line). Plotted is the astrophysical flux as a function of the energy. The models are for a $120 M_{\odot}$ track dwarf model with parameters: *CoStar*: model F2, Kunze: ($T_{\text{eff}}, \log g$) = (50 kK, 4.0) and Kurucz: ($T_{\text{eff}}, \log g$) = (50 kK, 5.0)

$\log g$ – $\log T_{\text{eff}}$ parameter space as the present *CoStar* calculations. The Kunze models include 9 of the most abundant elements in non-LTE (H, He, C, N, O, Ne, Mg, Al, Si, S and Ar). Grids for plane parallel non-LTE models, which also include iron are not yet available (e.g. Dreizler & Werner 1993, Hubeny & Lanz 1995).

120 M_{\odot} track

A comparison of models at the highest T_{eff} available (approximately O3 V stars) is shown in Fig. 5. Plotted is model F2 from the $120 M_{\odot}$ track (solid line), the Kunze model for ($T_{\text{eff}}, \log g$) = (50 kK, 4.0) and Kurucz’s model at ($T_{\text{eff}}, \log g$) = (50 kK, 5.0)³. While the Lyman continuum is essentially identical in all models, non-LTE effects increase the flux in the He I continuum in both non-LTE models (e.g. Mihalas & Auer 1970). Given the very large temperature, H and He are fully ionized and electron scattering becomes an important opacity source in the He I continuum. Consequently, wind effects have little influence on the EUV flux up to the He II continuum edge. Close to the He II edge, our model shows a small flux “ex-

³ At high temperatures the results from Kurucz models do not depend sensitively on gravity and should thus allow for an appropriate comparison.

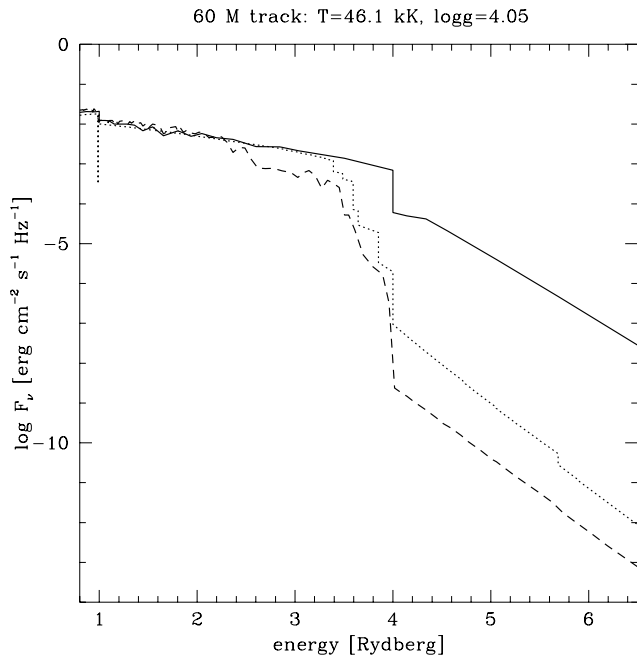


Fig. 6. Same as Fig. 5 for a $60 M_{\odot}$ dwarf. *CoStar*: model D2 (solid), Kunze (dotted): $(T_{\text{eff}}, \log g) = (45 \text{ kK}, 4.0)$ and Kurucz (dashed): $(T_{\text{eff}}, \log g) = (45 \text{ kK}, 5.0)$

cess” with respect to the model of Kunze (1994). This is probably due to lower blanketing above the C III and O III edges in our *CoStar* models (see Sect. 6). In the He II continuum, the wind model shows the strong characteristic flux increase due wind effects (Cases *a-iii* and *c-ii*).

60 M_{\odot} track

In Figures 6 and 7 we plot comparisons of dwarf and supergiant models from the $60 M_{\odot}$ track.

Dwarf model: Figure 6 shows the emergent flux for model D2 (solid line). It is compared to a model with $(T_{\text{eff}}, \log g) = (45 \text{ kK}, 4.0)$ from Kunze (dotted line) and a Kurucz model (dashed line) for $(45 \text{ kK}, 5.0)$. In the Lyman continuum all models yield essentially the same results. In the He I continuum, non-LTE effects increase the emergent flux. The slope of the continuum of our *CoStar* model is slightly flatter than that for the Kunze model (Case *a-ii*). This is also found in recent calculations of Sellmaier et al. (1996).

In the He II continuum the situation is a combination of Case *a-iii* and *c-ii*.

Supergiant model: The EUV flux distribution from the supergiant model (model D4 – but recalculated for $(T_{\text{eff}}, \log g) = (35 \text{ kK}, 3.2)$) is plotted in Fig. 7 (solid line). The comparison shows the corresponding plane parallel model from Kunze for identical T_{eff} and $\log g$ (dotted line) and a Kurucz model (dashed) with $(T_{\text{eff}}, \log g) = (35 \text{ kK}, 4.0)$. Given the strong stellar wind the ionizing flux is in-

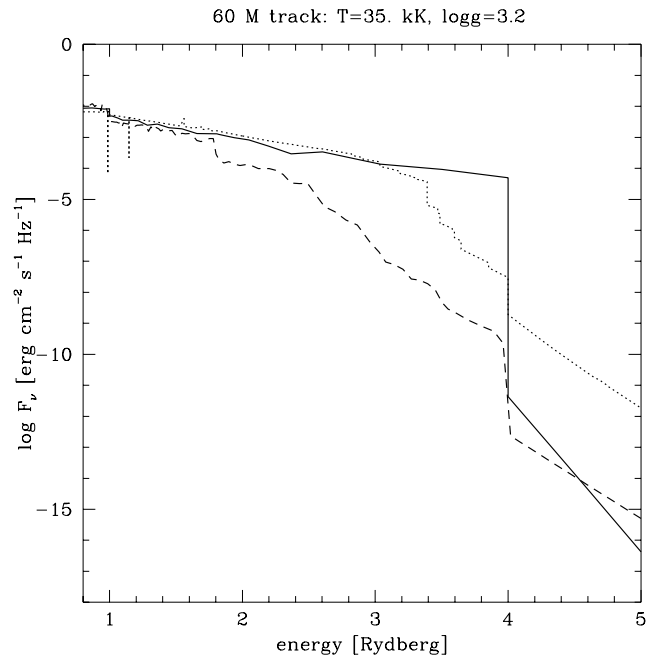


Fig. 7. Same as Fig. 5 for a $60 M_{\odot}$ supergiant. *CoStar*: model D4 (solid line). Parameters are as in Table. 1, except for $(T_{\text{eff}}, \log g) = (35 \text{ kK}, 3.2)$, Kunze (dotted): $(T_{\text{eff}}, \log g) = (35 \text{ kK}, 3.2)$, and Kurucz (dashed): $(T_{\text{eff}}, \log g) = (35 \text{ kK}, 4.0)$

fluenced by wind effects at essentially all wavelengths. As for the dwarf models, this leads to depopulated ground states (Case *a-iii*) but also causes the depth of continuum formation to be located in spherically extended layers. In this case the flattening of the spectrum in the He I continuum is mostly due to case (*b*). The spectrum up to the He II edge is flatter than plane parallel models. Due to stronger blanketing, the absolute flux in the Lyman continuum is lower than in the Kunze model. Above the He II edge the wind is optically thick up to large distances (Case *b*), which explains the low flux with respect to the plane parallel non-LTE model.

20 M_{\odot} track

The EUV spectra along the 40 and 25 M_{\odot} tracks are qualitatively identical to the ones discussed above although the differences with respect to plane parallel non-LTE models increase. For the least massive objects modeled with *CoStar*, however, the situation may be slightly different due to their relatively low mass loss rates.

Dwarf model: Figure 8 shows the dwarf model A1 (recalculated for $(T_{\text{eff}}, \log g) = (35 \text{ kK}, 4.0)$) compared to Kunze and Kurucz models with identical parameters. Due to stronger blanketing the Lyman continuum flux is slightly lower than the Kunze model.

Qualitatively the slope of the He I continuum resembles the cases discussed before. Figure 8, however, shows

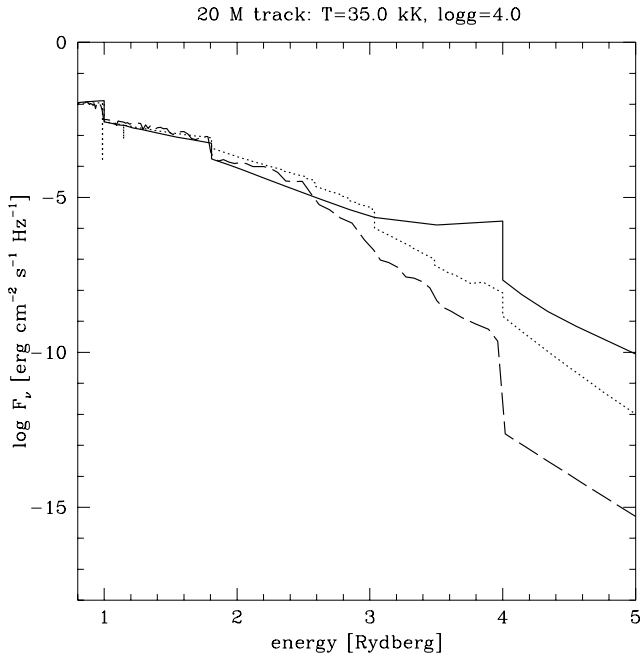


Fig. 8. Same as Fig. 5 for a $20 M_{\odot}$ dwarf. *CoStar* model A1 (solid line. Parameters as in Tab. 1 except $(T_{\text{eff}}, \log g) = (35 \text{ kK}, 4.0)$), Kunze (dotted) : $(T_{\text{eff}}, \log g) = (35 \text{ kK}, 4.0)$, and Kurucz (dashed) : $(T_{\text{eff}}, \log g) = (35 \text{ kK}, 4.0)$

that up to $\sim 2.6\text{--}3$ Rydberg the *CoStar* model predicts a flux lower than that in both the non-LTE and LTE plane parallel model. The difference relative to the Kunze model is clear example of a Case *a-ii* effect. A similar result was also obtained for $T_{\text{eff}} = 35 \text{ kK}$ by Sellmaier et al. (1996). Due to the weak wind, the flux increase in the He II continuum with respect to the plane parallel non-LTE model is not strongly pronounced (Case *a-iii*).

Giant models: Let us turn to the early B type giant models (Figure 9). This star has a relatively weak wind, however, the *CoStar* model shows surprisingly large differences when compared to plane parallel models. The cause for these large differences is not directly related to the outflow (the H I and He I continua are formed in the photosphere), but is a consequence of differences in temperature structure.

The temperature structures of model A4 and of the Kunze model for $(T_{\text{eff}}, \log g) = (25 \text{ kK}, 3.2)$ are given in the upper panel of Fig. 10. The lower panel shows the spherical extension of model A4. Note that the structures agree well at optical depths $\tau_{\text{Ross}} \gtrsim 1$. In the *CoStar* model the quasi-hydrostatic region reaches out to $\log \tau_{\text{Ross}} \sim -1.7$. At this point the wind flow starts to accelerate, causing the temperature to decrease rapidly. Given the weakness of the wind in the *CoStar* model, the intermediate region $-1.7 \lesssim \tau_{\text{Ross}} \lesssim 1$ where geometric extension is negligible is sufficiently large for the temperature to approach the value corresponding to that of the boundary temperature in a

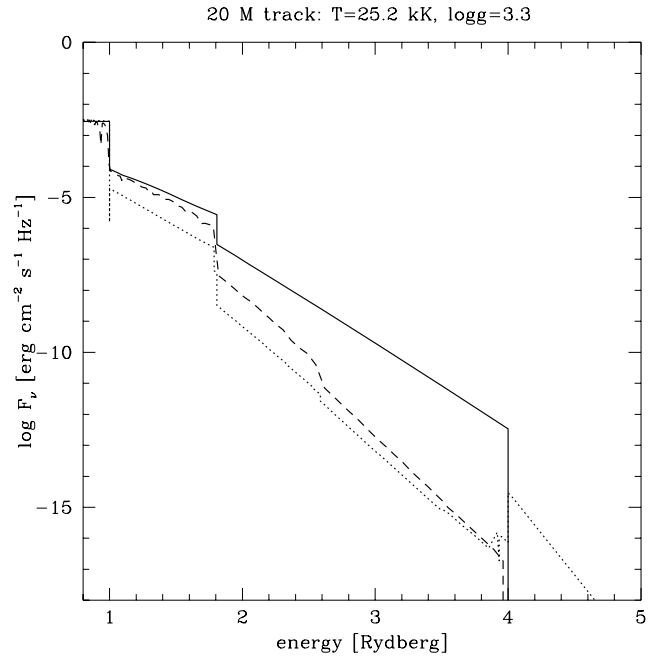


Fig. 9. Same as Fig. 5 for a $20 M_{\odot}$ supergiant. *CoStar* model A4 (solid line. Parameters as in Tab. 1), Kunze (dotted) : $(T_{\text{eff}}, \log g) = (25 \text{ kK}, 3.2)$, and Kurucz (dashed) : $(T_{\text{eff}}, \log g) = (25 \text{ kK}, 3.3)$

plane parallel grey atmosphere in radiative equilibrium, i.e. $T \rightarrow 0.841 T_{\text{eff}}$. At optical depths $\log \tau_{\text{Ross}} \lesssim -1.7$, the spherical extension makes itself known, leading to the rapid decline of the temperature.

As Fig. 10 shows, the temperature in the plane parallel non-LTE model is below the grey value, as expected, due to cooling of the metals. The difference with *CoStar* reaches up to $\sim 3500 \text{ K}$ close to the photosphere–wind transition zone, which is also the region where the He I and the Lyman continuum are formed (see Fig. 10). The higher temperature leads to a higher flux both in the Lyman and in the He I continuum of the *CoStar* model with respect to the Kunze model (see Fig. 9)⁴. The Kurucz model yields results intermediate between both non-LTE models. As discussed by Kunze (1994) this is due to an overestimation of the temperature gradient in the continuum forming layers in B star models of Kurucz (cf. Philips & Wright 1980).

In summary, we have seen that differences in the ionizing flux down to 228 \AA between *CoStar* models and plane parallel models become particularly large for the lowest mass tracks presented here. This is not what one would expect: Given the relatively low mass outflow of these objects, wind effects are expected to become less and less

⁴ In both models the H and He groundstates are overpopulated.

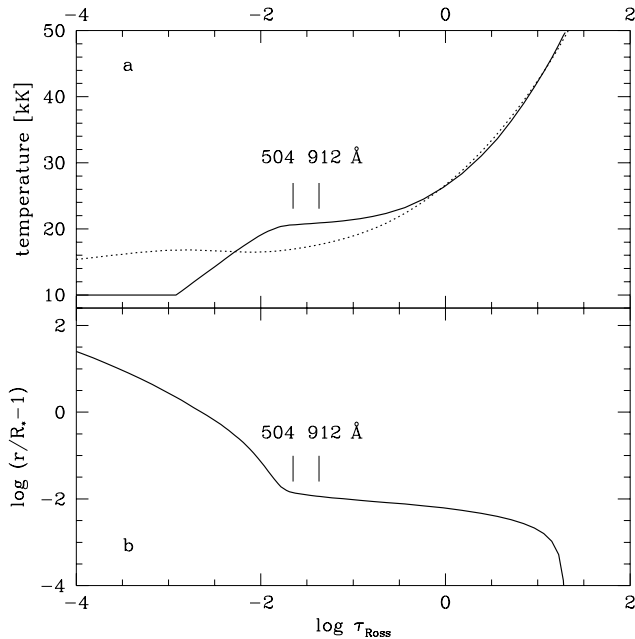


Fig. 10. **a** Comparison of temperature structures from model A4 (solid line) with a plane parallel non-LTE model of Kunze (1994) for $(T_{\text{eff}}, \log g) = (25 \text{ kK}, 3.2)$ (dotted). Also indicated are the depths of the He^o and Lyman continuum forming layers ($\tau_{\nu} = 2/3$) in the *CoStar* model A4. The temperature differences are discussed in the text. **b** Measure of the spherical extension of model A4. Plotted is $\log(r/R_{\star} - 1)$ as a function of the Rosseland optical depth. Note the location of the continuum forming layers in the photosphere–wind transition zone

important and the predictions should smoothly join those from non-LTE plane parallel models⁵.

But this does not occur. In fact the physical situation becomes more complex, as the temperature structure start to play an important role. Our predictions for BO dwarf and giant stars (roughly corresponding to models A) should thus be taken with caution. These uncertainties will be discussed in more detail in Sect. 6.

5. Revised ionizing fluxes of O and early B stars

In this section we present the integrated photon fluxes obtained from our models at solar and 1/5 solar metallicity and derive new calibrations for O3 to B0 stars of population I. We also compare our results with previous studies that use different atmosphere calculations.

⁵ Non-LTE effects are still of importance and one therefore does not expect the results to agree with the Kurucz models in this domain.

5.1. Integrated photon fluxes

In Table 2 we list the predicted number of photons emerging at wavelengths shorter than 912, 504, and 228 Å respectively, referred to as q_0 , q_1 , and q_2 . The values are given for both line blanketed models sets at $Z=0.020$ and 0.004 . The total ionizing luminosity Q_i (in photons s^{-1}) is obtained by $Q_i = 4\pi(R_{\star}R_{\odot})^2q_i$, where R_{\star} is given in Table 1.

The q_i values may be used to interpolate results for other stellar parameters and comparisons to predictions from plane parallel atmosphere models (cf. below). It must, however, be kept in mind that the fundamental value predicted by spherically extended models, such as the present ones, is the total ionizing luminosity (Q_i), since the radius is one of the basic model parameters. Using interpolations of q_i to obtain the number of ionizing photons for stars with significantly differing radii may therefore yield unreliable results. The same comment also applies to the wind parameters. Numerical care must be taken for interpolations since the model grid is not uniformly spaced in its input parameters. While reliable q_0 and q_1 interpolations can be done with 2-D surface interpolation algorithms the same is not true for q_2 , which shows a strong discontinuity in the $\log g - \log T_{\text{eff}}$ plane. For population synthesis applications the safest approach may be to assign the flux from some “nearest neighbour” model to the desired point and scale it to the correct bolometric luminosity, as mostly done.

5.2. Metallicity effects

As mentioned in Sect. 2.2.2, a change in metallicity basically affects our results in three different ways: 1) Change of the total metal abundance, 2) change of the relative hydrogen to helium abundances expected from the chemical evolution, and 3) modified wind properties due to 1). In Table 2 we give the ionizing photon fluxes derived from models at $Z=0.004$. These values are to be compared to the ones for solar metallicity.

In most cases the ionizing flux in the H and He I continuum increases with lower metallicity, as expected. The difference between both sets is, however, relatively small. Typically q_0 changes by less than $\sim 30\%$, although larger variations are found for q_1 . The main influence in our models results from effect 3), mentioned above. Effects 1) and 2) are of secondary importance. At $Z=0.004$ both the decrease of the wind velocities and the mass loss rate imply a diminishing importance of wind effects. Consequently, cascading from upper levels (case *a-ii*) becomes less important. Thus the H groundstate is less over-populated compared to the solar metallicity case, implying a slightly stronger flux in the Lyman continuum. Similar reasoning applies to the He I continuum for the temperature range covered in our models.

Table 2. Ionizing photon fluxes in $\text{cm}^{-2}\text{s}^{-1}$ from *CoStar* models at $Z=0.020$ (columns 2-4) and $Z=0.004$ (columns 5-7). For $Z=0.020$ the stellar parameters are given in Table 1. The low Z models include abundance changes as well as the expected variations of the wind parameters. Empty columns denote fluxes $< 10^3 \text{ cm}^{-2}\text{s}^{-1}$

model	Z=0.020			Z=0.004		
	log q_0	log q_1	log q_2	log q_0	log q_1	log q_2
20 M_{\odot} track:						
A1	23.63	22.12	18.27	23.73	22.33	18.75
A2	23.35	21.59		23.39	21.69	
A3	22.92	20.84		22.96	20.95	
A4	21.89	19.10		21.89	19.17	
25 M_{\odot} track:						
B1	24.04	23.25	20.14	24.10	23.33	20.03
B2	23.85	22.85	19.67	23.85	22.82	19.53
B3	23.33	21.50		23.36	21.57	
B4	22.52	20.09		22.52	20.08	
40 M_{\odot} track:						
C1	24.47	23.97	21.56	24.50	24.00	20.49
C2	24.33	23.75	21.27	24.35	23.80	20.69
C3	24.05	23.31	20.13	24.08	23.40	20.13
C4	23.00	20.84	8.69	23.23	21.25	
C5	22.38	19.95	6.27	22.43	19.76	
C6	20.90	14.02		20.75		
60 M_{\odot} track:						
D1	24.67	24.20	21.95	24.68	24.23	20.95
D2	24.58	24.09	21.54	24.60	24.13	20.79
D3	24.23	23.59	20.44	24.25	23.64	20.64
D4	23.64	22.48	12.42	23.64	22.50	11.49
D5	22.68	20.18	7.09	22.71	20.24	6.34
D6	21.65	15.59		21.65	18.16	
D7	21.74	15.62		21.82	18.34	
85 M_{\odot} track:						
E1	24.81	24.39	21.55	24.82	24.40	21.38
E2	24.71	24.25	21.49	24.72	24.27	21.27
E3	24.45	23.88	20.89	24.44	23.90	20.98
120 M_{\odot} track:						
F1	24.92	24.50	21.79	24.91	24.51	21.57
F2	24.80	24.35	21.74	24.80	24.37	21.55
F3	24.69	24.20	21.19	24.69	24.22	21.53

As discussed at length, the He II ionizing flux is most sensitive to wind effects. In general, a lowering of the metallicity implies a decrease of the wind density leading to less emission in the He II continuum. However, in some cases of stars with large wind densities (e.g. models E3 and F3) the opposite is seen. This is similar to what is seen in hot Wolf-Rayet stars: The He II continuum is formed at a relatively large radius, where the ground state population drives the ionization, making it proportional to the total density (e.g. Schmutz & Hamann 1986). In this situation lowering the wind density (i.e. lowering Z) reduces the recombination rates, implying a stronger ionization.

This explains the increase of the He II ionizing flux for the models with the highest wind densities when lowering the metallicity⁶. In summary, we see that the metallicity dependence of the ionizing fluxes predicted by our models is relatively small and essentially due to the expected changes of the wind properties with Z (effect 3)). However, given the likely underestimate of blanketing in our models (see Sect. 6) we expect the dependence on metal abundances to be somewhat more important than found here.

5.3. A new ionizing flux calibration for O3–B0 stars

Recently Vacca et al. (1996) derived new calibrations of stellar parameters for O3 to B0.5 stars. These are based on results from detailed modeling of the observed absorption line spectra of stars with well-defined spectral classifications. Using these calibrations Vacca et al. (1996) calculate ionizing photon fluxes in the H and He^o continua based on Kurucz (1991) LTE model atmospheres⁷. In view of the important improvements included in our *CoStar* models, it is of particular interest to provide a recalibration of the photon fluxes taking into account non-LTE and wind effects and line blanketing.

Table 3 shows our new calculations of the H and He I ionizing fluxes for O3 to B0.5 stars of luminosity classes V, III, and I. Given are the photon fluxes per unit surface q_0 and q_1 . We also provide absolute photon fluxes Q_0 and Q_1 , adopting the radii from the recent calibration of Vacca et al. (1996) in Table 3. The photon fluxes have been derived from our solar metallicity models (Table 2) using a two-dimensional surface interpolation routine based on a modified Shepard method (NAG `e01sef` routine). For the reasons mentioned above we have refrained from interpolating values for the He II ionizing fluxes. The $\log q_i$ values have been interpolated in the $\log g - \log T_{\text{eff}}$ plane. For the gravity calibration we prefer to use the “evolutionary gravity” g_{evol} given by Vacca et al., since these values are consistent with the gravity definition in our *CoStar* models. Furthermore the distinction with their “spectroscopic gravity” is not of great concern for the comparison with the ionizing fluxes since their values are only weakly dependent on the adopted gravity (see below).

⁶ In model F3 the He enrichment further augments this behaviour.

⁷ For clarification a brief comment on the procedure of Vacca et al. (1996) for deriving Kurucz ionizing fluxes appears useful: As shown in Fig. 1 the Kurucz (1991) models only cover the domain of the 20 and 25 M_{\odot} track. It is important to note that for the rest of the domain of interest, which corresponds to all O3 to O9 stars, extrapolations combined with blackbody spectra are used to extend the Kurucz grid to the desired lower gravities.

Table 3. Parameters for OB-type stars: Ionizing photon fluxes per unit surface area (q_0 and q_1 in column 4 and 5) derived from solar metallicity *CoStar* models, using the $T_{\text{eff}}\text{--}\log g$ calibration of Vacca et al. (1996) given in columns 2 and 3. Adopting the radii from Vacca et al. (column 4) one obtains the absolute photon fluxes Q_0 and Q_1 given in column 5 and 6

Sp. Type	T_{eff} [K]	$\log g_{\text{evol}}$ [cgs]	$\log q_0$ [$\text{cm}^{-2}\text{s}^{-1}$]	$\log q_1$ [$\text{cm}^{-2}\text{s}^{-1}$]	R [R_{\odot}]	$\log Q_0$ [s^{-1}]	$\log Q_1$ [s^{-1}]
Luminosity class V:							
O3 V	51230.	4.149	24.82	24.39	13.2	49.85	49.42
O4 V	48670.	4.106	24.71	24.27	12.3	49.68	49.23
O4.5 V	47400.	4.093	24.65	24.20	11.8	49.58	49.12
O5 V	46120.	4.081	24.58	24.11	11.4	49.48	49.01
O5.5 V	44840.	4.060	24.51	24.00	11.0	49.38	48.86
O6 V	43560.	4.042	24.44	23.91	10.7	49.28	48.75
O6.5 V	42280.	4.030	24.36	23.81	10.3	49.17	48.62
O7 V	41010.	4.021	24.27	23.65	10.0	49.05	48.44
O7.5 V	39730.	4.006	24.18	23.50	9.6	48.93	48.25
O8 V	38450.	3.989	24.08	23.33	9.3	48.80	48.05
O8.5 V	37170.	3.974	23.94	23.05	9.0	48.64	47.74
O9 V	35900.	3.959	23.79	22.70	8.8	48.46	47.37
O9.5 V	34620.	3.947	23.60	22.27	8.5	48.25	46.92
B0 V	33340.	3.932	23.40	21.79	8.3	48.02	46.41
B0.5 V	32060.	3.914	23.18	21.27	8.0	47.77	45.86
Luminosity class III:							
O3 III	50960.	4.084	24.81	24.37	15.3	49.97	49.52
O4 III	48180.	4.005	24.70	24.24	15.1	49.84	49.38
O4.5 III	46800.	3.971	24.64	24.18	15.0	49.78	49.32
O5 III	45410.	3.931	24.58	24.11	15.0	49.71	49.25
O5.5 III	44020.	3.891	24.51	24.03	14.9	49.64	49.16
O6 III	42640.	3.855	24.43	23.92	14.8	49.56	49.05
O6.5 III	41250.	3.820	24.34	23.78	14.8	49.47	48.91
O7 III	39860.	3.782	24.24	23.63	14.7	49.36	48.75
O7.5 III	38480.	3.742	24.12	23.41	14.7	49.24	48.53
O8 III	37090.	3.700	23.97	23.03	14.7	49.09	48.14
O8.5 III	35700.	3.660	23.82	22.68	14.7	48.94	47.80
O9 III	34320.	3.621	23.64	22.28	14.7	48.76	47.40
O9.5 III	32930.	3.582	23.44	21.83	14.7	48.56	46.95
B0 III	31540.	3.542	23.21	21.35	14.7	48.33	46.47
B0.5 III	30160.	3.500	22.98	20.90	14.8	48.11	46.03
Luminosity class I:							
O3 I	50680.	4.013	24.81	24.34	17.8	50.09	49.63
O4 I	47690.	3.928	24.69	24.24	18.6	50.02	49.56
O4.5 I	46200.	3.866	24.63	24.19	19.1	49.98	49.53
O5 I	44700.	3.800	24.57	24.10	19.6	49.94	49.47
O5.5 I	43210.	3.740	24.49	23.96	20.1	49.88	49.35
O6 I	41710.	3.690	24.40	23.83	20.6	49.81	49.24
O6.5 I	40210.	3.636	24.30	23.69	21.2	49.73	49.12
O7 I	38720.	3.577	24.18	23.45	21.8	49.64	48.91
O7.5 I	37220.	3.516	24.05	23.17	22.4	49.53	48.65
O8 I	35730.	3.456	23.91	22.86	23.1	49.42	48.37
O8.5 I	34230.	3.395	23.75	22.52	23.8	49.29	48.05
O9 I	32740.	3.333	23.55	22.11	24.6	49.12	47.67
O9.5 I	31240.	3.269	23.31	21.61	25.4	48.90	47.21

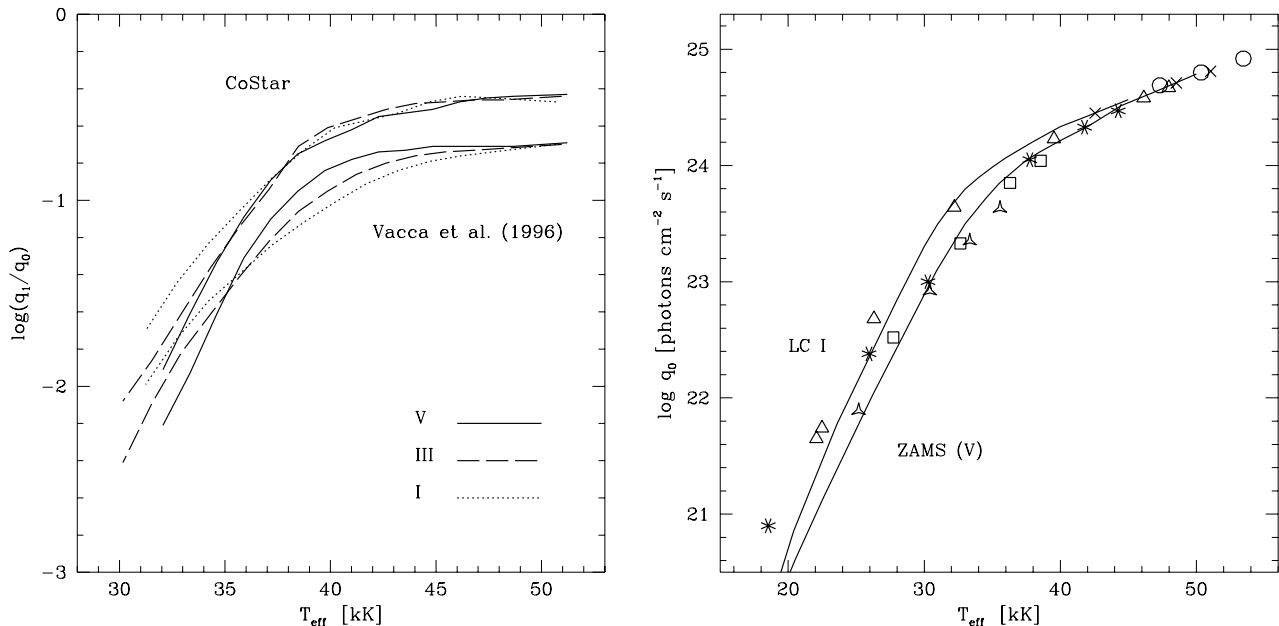


Fig. 11. Left panel: Logarithm of the hardness ratio $\log(q_1/q_0)$ as a function of effective temperature for dwarfs, giants and supergiants. Shown are the values from our *CoStar* models (see Table 3) and those derived by Vacca et al. (1996) using Kurucz models. **Right panel:** Logarithm of the number of Lyman continuum ionizing photons versus effective temperature. The predictions from our models are plotted using the same symbols as in Fig. 1. The solid lines shows the relations from Panagia (1973) for his ZAMS and luminosity class I

5.4. Comparison with previous calibrations

We compare our results from Table 3 with those derived by Vacca et al. (1996) using the Kurucz (1991) models. A brief comparison with earlier work of Panagia (1973) will also be given.

For all O3 to B0.5-type stars, the total number of *Lyman continuum photons* q_0 is somewhat *lower* than predicted by the Kurucz models. The difference increases from 0.03 to 0.07 dex ($\sim 7\%$ to 15%) between O3 and O7 respectively. For later types this behaviour increases strongly and reaches 0.14 (0.26) dex for B0 dwarfs (O9.5 supergiants). More important is the comparison with the He I photon flux, which is strongly affected by non-LTE and wind effects (see above). For the dwarf sequence in Table 3, q_1 is *larger* by ~ 25 to 75% with respect to the values presented by Vacca et al. For supergiants q_1 is typically increased by a factor of 2. It has already been noted by Vacca (1994) and by Vacca et al. (1996) that the q_1 values based on Kurucz models should be systematically underestimated because of the assumption of LTE.

As mentioned in Sect. 4.1, our results for the latest spectral types do neither smoothly tend towards the Kurucz values, nor do they tend to the results of the plane parallel non-LTE models of Kunze (1994). Model calculations for later types will be necessary to locate more precisely where non-LTE and wind effects become negligible (but see Sect. 6). Since for most applications involv-

ing H II regions and alike systems the ionizing spectrum will be determined by the most massive stars present, the presence of the “discontinuity” will not be of importance.

In Figure 11 (left panel) we plot the hardness ratio q_1/q_0 from the *CoStar* values of Table 3 as a function of T_{eff} . Also shown is the hardness ratio derived by Vacca et al. As pointed out by these authors (cf. also Vacca 1994), it must be kept in mind that these values should be higher by typically a factor of 2 if one accounted for non-LTE effects in plane parallel models. Figure 11 clearly shows the overall increase of the hardness of the ionizing spectrum at a given temperature. The strongest hardening is found for supergiants due to the increasing importance of wind effects. Interestingly, for stars with $T_{\text{eff}} \gtrsim 36000$ K we find that the hardness ratio is essentially independent of luminosity class while the values of Vacca et al. show a spread of up to ~ 0.2 dex. To produce a hardness ratio of $\log(q_1/q_0) < -0.7$ with our new models the temperature of the exciting star can be ~ 1000 to 11000 K smaller than if Kurucz models were used. Therefore the general tendency is that lower effective temperatures would be derived from observed nebular properties if one uses atmosphere models, which account for non-LTE, line blanketing and stellar winds.

Finally it is interesting to make a brief comparison with the widely used results of Panagia (1973). For further comparisons see Vacca et al. Figure 11 (right panel)

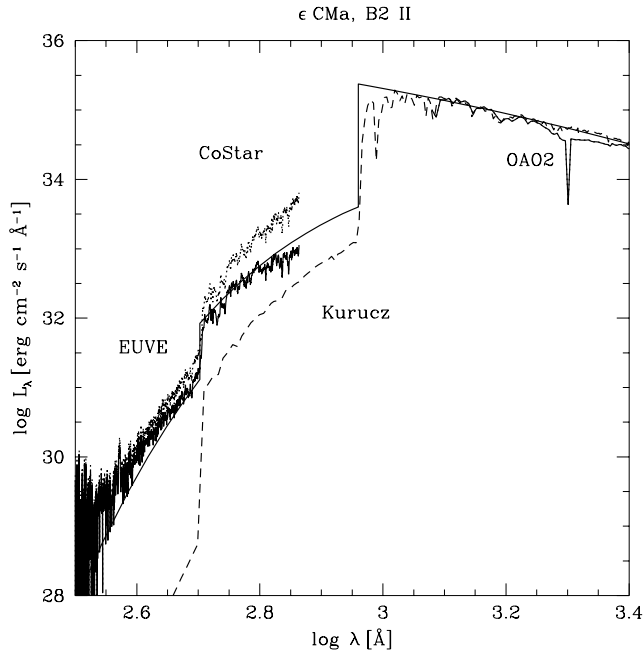


Fig. 12. Far UV and EUV flux of ϵ CMa. EUVE observations from Cassinelli et al. (1995) corrected for an attenuation by $N_{\text{HI}} = 1.10^{18}$ (dotted line up to ~ 700 Å) and $N_{\text{HI}} = 5.10^{17}$ cm $^{-2}$ (Gry et al. 1995; solid line) Model comparisons: *CoStar* model (solid line, Parameters from Table 4), Kurucz model (dashed) with $(T_{\text{eff}}, \log g) = (21 \text{ kK}, 3.0)$. All fluxes are scaled (consistently with R_*) to the distance of 188 pc. Discussion in text

shows the comparison of the number of Lyman continuum photons between Panagia and our *CoStar* models. The behaviour of the models from the 40, 60, and 85 M_{\odot} track has already been discussed in Paper II. The figure clearly illustrates the smaller *CoStar* Lyman continuum flux for the dwarfs at $T_{\text{eff}} \lesssim 40$ kK which was also apparent in the above comparison with Vacca et al. The same also holds for the evolved stars from the 20 and 25 M_{\odot} tracks. The models with values of q_0 larger than the supergiants of Panagia are the extreme supergiant models from the 40 and 60 M_{\odot} track.

6. Discussion

We have shown that our models provide an important improvement describing the ionizing fluxes of hot stars. However, it is also important to discuss possible shortcomings in our method, which may affect our results. As discussed in Sects. 2.1 and 4.1 the uncertainties in our models are expected to become increasingly important for B stars, which have weak winds. This can be easily understood and it is best illustrated by considering the following brief exploratory study of two unique cases of B2 giants, which have recently been observed shortward of the Lyman limit with EUVE.

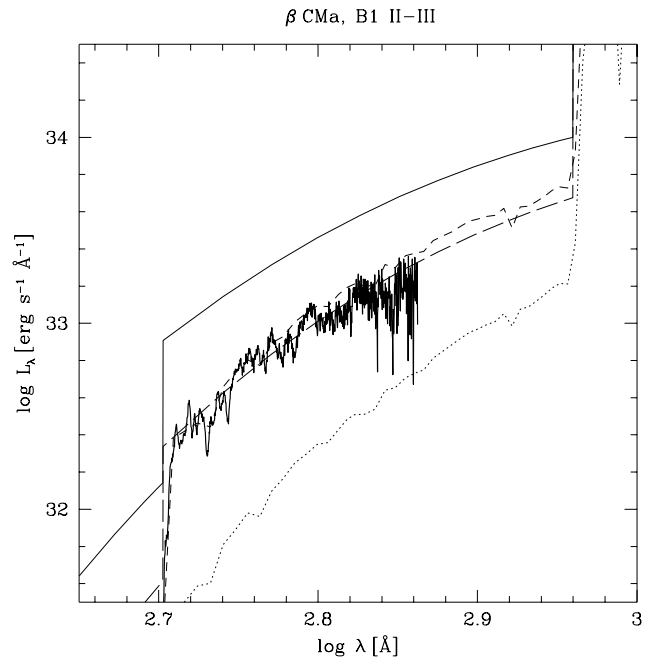


Fig. 13. EUV flux of β CMa. EUVE observations from Cassinelli et al. (1996) corrected for an attenuation by $N_{\text{HI}} = 2.10^{18}$ cm $^{-2}$ (solid line up to ~ 700 Å). The following models are shown for comparisons: *CoStar* models (Parameters from Table 4. Solid line: hot model ; long-dashed: cooler model), Kurucz models with $(T_{\text{eff}}, \log g) = (25 \text{ kK}, 3.5)$ (dashed) and $(23 \text{ kK}, 3.5)$ (dotted). All fluxes are scaled (consistently with R_*) to the distance of 206 pc. Discussion in text

6.1. Comparisons with EUVE observations

The first EUV spectra from early type stars have been observed by Hoare et al. (1993). Subsequent EUVE observations of ϵ CMa (B2II) and β CMa (B1 II–III) by Cassinelli et al. (1995, 1996), have provided spectra allowing detailed comparisons with model atmospheres. As mentioned before, these observations have revealed important discrepancies with predictions from plane parallel model atmospheres. Najarro et al. (1996) have pointed out that these shortcomings could, at least partly, be explained by models which account for stellar winds. Their invoked mechanism is that of Case *a-iii* working in the He I continuum. This is the same mechanism that is relevant in the He II continua of the O-type star models discussed here. It is therefore interesting to see how well our predictions agree, notwithstanding the fact that the stellar parameters of ϵ and β CMa lie somewhat outside of the temperature domain covered in this work.

6.1.1. ϵ CMa

The adopted stellar parameters for ϵ and β CMa are given in Table 4. Temperature, gravity and radius are from Cassinelli et al. (1995). We assume solar abundances. The

wind parameters of ϵ CMa are somewhat uncertain. The adopted mass loss rate for ϵ CMa is compatible with the studies of Drew et al. (1994), Cassinelli et al. (1995) and Najarro et al. (1996). The same v_∞ and β as assumed by Najarro et al. are chosen to allow for a comparison with their work.

Table 4. Stellar parameters for ϵ and β Canis Majoris

	ϵ CMa	β CMa
T_{eff} [kK]	21.0	(24.8, 23.25)
$\log g$ [cgs]	3.2	(3.7, 3.4)
R_* [R_\odot]	16.2	11.54
n_{H}	0.9	0.9
\dot{M} [$M_\odot \text{yr}^{-1}$]	1.10^{-8}	3.510^{-8}
v_∞ [km s^{-1}]	800.	1220.
β	1.	1.

The spectral energy distribution predicted by *CoStar* and the one observed are given in Fig. 12. The result from a Kurucz model (dashed line) for $(T_{\text{eff}}, \log g) = (21 \text{ kK}, 3.0)$ plotted for comparison. The dotted line shows the observed EUVE flux corrected for a hydrogen column density $N_{\text{HI}} = 1.10^{18} \text{ cm}^{-2}$ (cf. Cassinelli et al. 1995). The solid line shows the observation corrected using the recently derived value of $N_{\text{HI}} = 5.10^{17}$ (Gry et al. 1995). The comparison with the plane parallel LTE model illustrates the striking underestimate of the continuum flux in both the Lyman and the He I continuum. As pointed out by Cassinelli et al., the finding of an observed “EUV excess” holds for any plane parallel model, i.e. it is independent of the assumption of LTE or non-LTE.⁸ As the figure shows, our model atmosphere yields a stronger EUV emission which significantly improves the comparison with the observations.

Does this result solve the “EUV excess” problem in ϵ CMa? The answer is: *no*. To explain this conclusion we need to identify the reason(s) for the EUV increase in our model relative to that of the plane parallel model. There are two basic reasons:

The first and major reason is simply a larger temperature in the continuum forming layers of our *CoStar* model. Indeed, in our model the temperature at the depth of continuum formation at $\lambda \sim 600 \text{ \AA}$ is $T \simeq 17 \text{ kK}$, which is larger than the value in the Kurucz model ($T \simeq 14 \text{ kK}$, Cassinelli et al. 1995). Although the ground states of H and He are slightly overpopulated in this region, the net result is nevertheless a stronger EUV emission. In fact, the structure of our model qualitatively resembles the structure of model A4 plotted in Fig. 10. The considered continuum forming layers are located at small optical depths

⁸ Non-LTE effects even decrease the EUV flux for the parameters of interest.

($\log \tau_{\text{Ross}} \lesssim -2$), where the temperature drop due to the spherical extension has not yet set in and the temperature is thus close to the boundary value of the plane parallel grey atmosphere. This explains the relatively high temperature. As for model A4, discussed in Sect. 4.1, we therefore conclude that the EUV emission is strongly dependent on the temperature structure in the transition zone between photosphere and wind.

The second reason regards the treatment of line broadening and its effect on the amount of line blanketing. In the present calculations for ϵ and β CMa, line blanketing turns out to be essentially ineffective. This unrealistic behaviour is due to the neglect of line broadening (cf. below). Introducing a small “turbulent” line broadening using the simple method of Schaerer & Schmutz (1992) results in a significant decrease of the EUV flux. This further points out the need for an improved treatment of line blanketing for later type stars with weak stellar winds.

Najarro et al. (1996) have pointed out the importance of the stellar wind on the ground state populations of H and He and hence on the emergent EUV flux of early B giants. To compare our models with their results we calculated a series of models where we varied the mass loss rate from 10^{-9} to $10^{-6} M_\odot \text{yr}^{-1}$, keeping all other parameters as in Table 4. We do not confirm their strong dependence of the model fluxes on mass loss. In particular we obtain a much weaker dependence of the Lyman jump, the He I jump and the number of ionizing photons on mass loss. This finding is confirmed by comoving frame calculations (Schmutz 1995, private communication). Our results thus indicate that the strong mass loss dependence of the EUV flux found by Najarro et al. must be partly due to variations of their temperature structure with \dot{M} . The amplitudes of these variations seem significantly larger than those in our calculations. This may originate from their simplified energy equation (they assume radiative equilibrium accounting only for H and He), which is used to derive their temperature structure. This finding stresses the importance of deriving both reliable temperature structures and accurate non-LTE populations including a detailed treatment of line blanketing and stellar winds to obtain reliable ionizing fluxes for B stars.

6.1.2. β CMa

The adopted stellar parameters for β CMa are given in Table 4. Given the ambiguity of these parameters (Cassinelli et al. 1996), we present two *CoStar* models corresponding to the limiting cases discussed by Cassinelli et al. For the wind parameters we also follow these authors and adopt their theoretical estimates based on the modified CAK theory. As for ϵ CMa we assume solar abundances.

The predicted spectra and the *EUVE* observations are compared in Fig. 13. The solid and long-dashed lines show the results from the hotter and cooler *CoStar* model respectively. Kurucz model predictions for comparable pa-

rameters (see figure caption) are shown as short-dashed and dotted lines. Compared to the Kurucz models, our calculations again show a stronger EUV flux for a given T_{eff} . Similar to the ϵ CMa model discussed above, this is mostly due to a temperature difference in the continuum forming layer as the ground state of H is overpopulated.

The *CoStar* model with the lower T_{eff} (23250 K) fits the *EUVE* observations best. Interestingly, this effective temperature was favoured by Cassinelli et al. (1996) based on a comparison of the UV to near-IR flux distribution. In this case, the EUV emission predicted by the Kurucz model is considerably too weak. Our results thus show that even for the low T_{eff} value and despite non-LTE effects, which overpopulate the ground state, the observed EUV flux can be reproduced with the temperature structure from our models. As for ϵ CMa, the key questions are again: how realistic is this structure, and more fundamentally, what are the physical processes that establish such a temperature structure?

6.2. Current approximations and future improvements

The exploratory results in the previous section clearly show that for stars of spectral types later than approximately B0 (not covered by our grid) reliable predictions of ionizing fluxes are not yet possible. Therefore we have limited our model set to O3–B0 stars. We shall now briefly discuss the most important model assumptions and their importance for the set of calculations presented in Table 1. The assumptions listed in Sect. 2.1 will be addressed in the following.

The Sobolev approximation, which is made for the line transfer should yield sufficiently precise results for the parameters of our model set (see also de Koter et al. 1993). The weakest point in our Monte-Carlo treatment of line blanketing is most likely the neglect of line broadening, yielding only a poor treatment of photospheric lines (see Paper II). Line blanketing in the low velocity part of the atmosphere is therefore underestimated in the present models. Although we have presently no possibility to quantify the importance of photospheric blanketing, we expect that our results should be fairly reliable for the O stars for the following reasons: 1) photospheric lines are both weaker and less numerous than in later types, and 2) given their strong outflow, wind effects play a dominant role in establishing the equilibrium population.

A characteristic feature of the line blanketed non-LTE models of Kunze (1992, 1994) is the appearance of relatively strong absorption edges in the He I continuum which are mostly due to CNO, but also due to Ne and Ar (see e.g. Figs. 7, 8). These edges are not treated in our calculations. The Kunze models, on the other hand, do not include lines of iron peak elements, which are treated in our calculations, and which cause an important fraction of the metal line blanketing. Recently Sellmaier et al. (1996) presented calculations which include line blocking and

non-LTE effects in a stellar wind model. We note that their exploratory results also lack of pronounced metal ionization edges in the EUV, which seems to confirm our calculations. A more detailed analysis of this question will be possible with the inclusion of additional metals in the full non-LTE calculations (see e.g. de Koter et al. 1994, 1996a).

A potential source of uncertainty for high T_{eff} models could come from the coherent treatment of electron scattering, which might modify the He ionization, as pointed out by Rybicki & Hummer (1994). This effect remains to be included in future models.

As discussed in Paper II, the high energy part of the spectrum may be affected by the emission of X-rays which are usually attributed to shocks in the stellar winds. We did not include such shocks in our calculations. This may cause us to underestimate the flux in the He⁺ continuum. At longer wavelengths, our results should hardly be affected by X-rays as shown by the work of MacFarlane et al. (1994). They find that X-rays cause only a small perturbation of the wind structure in the O-type stars discussed in this paper. For stars of later spectral types the situation is different. For these stars, which have relatively weak winds, they do find that X-rays may drastically alter the wind ionization and possibly also contribute to heating in the photosphere. For the understanding of later types than those included in our sets, and particularly for an explanation of the “EUV excess” of ϵ and β CMa (cf. Sect. 6.1), the inclusion of X-rays will probably be of great concern.

7. Summary and conclusions

The present work provides an extensive set of predictions regarding the spectral energy distribution of massive stars ($M_1 = 20$ to $120 M_{\odot}$) derived from our combined stellar structure and atmosphere models. Our set covers the entire main sequence evolution and approximately corresponds to O3–B0 stars of all luminosity classes. This represents the first set of predictions for O and early-B stars, which are based on the most recent atmosphere models accounting for non-LTE effects, line blanketing, and stellar winds. Especially the treatment of the stellar wind is found to be of great importance for predicting reliable ionizing fluxes of hot stars. Our calculations should provide, for the first time, a reliable description of the spectral energy distribution in the He I and He II continuum, where non-LTE, line blanketing, and wind effects are crucial.

We have discussed the importance of wind effects and line blanketing in O3 to B0 stars in relation to the predicted ionizing fluxes. As already partly found in previous investigations (Gabler et al. 1989, 1992; Schaerer 1995, Najarro et al. 1996, Schaerer et al. 1996a, b) these effects have a profound importance on shaping the EUV flux of hot MS stars. The main conclusions can be summarised as follows:

- For stars with $T_{\text{eff}} \gtrsim 35$ kK the flux in the He II continuum is increased by 2 to 3 orders of magnitudes compared to predictions from non-LTE plane parallel model atmospheres (cf. Gabler et al. 1989). With respect to Kurucz LTE models there is a 3-6 orders of magnitude increase at $T_{\text{eff}} \gtrsim 38000$ K.
- The flux in the He I continuum is not only increased due non-LTE effects (e.g. Kudritzki et al. 1991) but is also modified by wind effects (cf. Najarro et al. 1996, Paper II). The combined effect of the mass outflow and line blanketing lead to a *flatter energy distribution* in the He I continuum (see also Sellmaier et al. 1996). Typically our models lead to an increase of a factor of 1.25 to 2 for the He I ionizing photon flux with respect to Kurucz models.
- The Lyman continuum fluxes are modified due to line blanketing and stellar winds, although to a lesser degree than the spectrum at higher energies. For most cases the differences with Kurucz models are less than ~ 20 % in the ionizing photon flux.

Using our calculations we provide revised ionizing fluxes for O3 to B0 stars (see Sect. 5) based on the recent temperature and gravity calibrations of Vacca et al. (1996). The total number of Lyman continuum photons is found to be slightly lower than those of Vacca et al., which are derived from the plane parallel LTE models of Kurucz (1991). Due to the increased flux in the He I continuum, the hardness ratio q_1/q_0 of the He I to H I continuum is increased by factors of ~ 1.6 to ~ 2.5 depending on spectral type and luminosity class. These high hardness ratios only follow from Kurucz models at temperatures of about 1000 to 11000 kK higher than used in our models.

We have discussed the assumptions inherent in our models and point out future improvements. These improvements will be especially important for understanding the EUV spectra of B-type stars, which show relatively weak stellar winds. We have analysed the EUV spectra of the recently observed B giants ϵ and β CMa (Cassinelli et al. 1995, 1996) and have shown that reliable calculations of the temperature structure in a model accounting for the stellar wind and which includes a detailed treatment of photospheric blanketing will be crucial to reproduce the EUVE observations. We argue that these effects are likely more important than the pure wind effect invoked by Najarro et al. (1996) to explain the EUV excess of ϵ CMa (Sect. 6.1).

Although potential shortcomings have been identified (Sect. 6), we consider our predictions to be fairly reliable for O stars (see also Schaerer 1996). The recent study of Sellmaier et al. (1996) shows that H II regions can provide very sensitive tests and that their exploratory models, which are similar to the present ones, are quite successful in explaining the observations. To explore the broader impact of our new ionizing fluxes a grid of H II region models has been calculated using the nebular photoionization

code *PHOTO* of Stasińska (see Stasińska & Schaerer 1996, Leitherer et al. 1996).

The spectral energy distributions are available on request from the authors and will be included in a forthcoming AAS CD-ROM (Leitherer et al. 1996).

Acknowledgements. DS particularly thanks André Maeder for his encouragement and support for this project. Dietmar Kunze kindly provided results from his atmosphere calculations. EUVE observations were made available by David Cohen. DS also thanks Bill Vacca, Werner Schmutz and Jacques Babel for numerous discussions and comments. This work was supported in part by the Swiss National Foundation of Scientific Research and by NASA through contract NAS5-31842.

References

- Auer L.H., Mihalas D., 1972, ApJS 24, 193
 Anders E., Grevesse N., 1989, Geochim. Cosmochim. Acta 53, 197
 Cassinelli J.P., Cohen D.H., MacFarlane J.J., Drew J.E., Lynas-Gray A.E., Hoare M.G., Vallerger J.V., Welsh B.Y., Vedder P.W. Hubeny I., Lanz T., 1995, ApJ 438, 932
 Cassinelli J.P., Cohen D.H., MacFarlane J.J., Drew J.E., Lynas-Gray A.E., Hubeny I., Vallerger J.V., Welsh B.Y., Hoare M.G., 1996, ApJ 460, 949
 Charbonnel C., Meynet G., Maeder A., Schaller G., Schaerer D., 1993, A&AS 101, 415
 de Jager C., Nieuwenhuijzen H., van der Hucht K.A., 1988, A&A 173, 293
 de Koter A., 1993, Ph.D. thesis, Univ. Utrecht
 de Koter A., Schmutz W., Lamers H.J.G.L.M., 1993, A&A 277, 561
 de Koter A., Heap S.R., Hubeny I., 1996a, ApJ, in press
 de Koter A., Hubeny I., Heap S.R., Lanz T., 1994 ApJ 435, L71
 de Koter A., Lamers H.J.G.L.M., Schmutz W., 1996b, A&A 306, 501
 Dreizler S., Werner K., 1993, A&A 278, 199
 Drew J.E., Denby M., Hoare M.G., 1994, MNRAS 266, 917
 Friend D.B., Abbott D.C., 1986, ApJ 311, 701
 Gabler R., Gabler A., Kudritzki R.P., Puls J., Pauldrach A., 1989, A&A 226, 162
 Gabler R., Kudritzki R.P., Mendez R.H., 1991, A&A 245, 587
 Gabler R., Gabler A., Kudritzki R.P., Mendez R.H., 1992, A&A 265, 656
 Groenewegen M.A.T., Lamers H.J.G.L.M., 1991, A&AS 88, 625
 Gry C., Lemonon L., Vidal-Madjar A., Lemoine M., Ferlet R. 1995, A&A 302, 497
 Hoare M.G., Drew J.E., Denby M., 1993, MNRAS 262, L19
 Hubeny I., Lanz T., 1995, ApJ 439, 875
 Hubeny I., Lanz T., 1996, in “Astrophysics in the Extreme Ultraviolet”, IAU Coll. 152, Eds. S. Bowyer, R.F. Malina, Kluwer, Dordrecht, p. 381
 Johnson H.L., 1966, ARA&A 4, 193
 Kudritzki R.P., 1988, in: Radiation in Moving Gaseous Media, 18th Advanced Course, Swiss Society for Astrophysics and Astronomy, Eds. Y. Chmielewski, T. Lanz, Geneva Observatory
 Kudritzki R.P., Pauldrach A., Puls J., 1987, A&A 173, 293

- Kudritzki R.P., Pauldrach A., Puls J., 1991b, in *The Magellanic Clouds*, IAU Symp. 148, Eds. R.Haynes, D.Milne, Kluwer Acad. Publ. p. 279
- Kunze, D., 1994, PhD thesis, Ludwig-Maximilians-Universität, Munich, Germany
- Kunze, D., Kudritzki R.P., Puls, J., 1992, in “The Atmospheres of Early Type Stars”, Eds. U. Heber, C.S. Jeffery, Lecture Notes in Physics 401, Springer–Verlag, p. 45.
- Kurucz R.L., 1991, in “Stellar Atmospheres: Beyond Classical Models”, NATO ASI Series C, Vol. 341, Eds. L.Crivellari, I.Hubeny, D.G.Hummer, p. 441
- Koornneef J., 1983, *A&A* 128, 84
- Lamla E., 1982, in *Landolt-Börnstein, New Series, Group IV, Vol. 2b*, Eds. K. Schaifers & H.H. Voigt, Springer, Berlin, p. 35
- Leitherer C., Robert C., Drissen L., 1992, *ApJ* 401, 596
- Leitherer C. et al., 1996, *PASP*, in press
- Lucy L.B., 1971, *ApJ* 163, 95
- MacFarlane J.J., Cohen D.H., Wang P., 1994, *ApJ* 437, 351
- Maeder A., Meynet G., 1994, *A&A*, 287, 803
- Meynet G., Maeder A., Schaller G., Schaerer D., Charbonnel C., 1994, *A&AS* 103, 97
- Mihalas D., Auer L.H., 1970, *ApJ* 160, 1161
- Najarro F., Kudritzki R.P., J.P. Cassinelli. O. Stahl, Hillier D.J., 1996, *A&A* 306, 892
- Panagia N., 1973, *AJ* 78, 929
- Pauldrach A., Puls J., Kudritzki R.P., 1986, *A&A* 164, 86
- Philips A.P., Wright S.L., 1980, *MNRAS* 192, 197
- Rubin R.H., Kunze D., Yamamoto T., 1995, in “Astrophysical Applications of Powerful New Atomic Databases”, ASP Conf. Series Vol. 78, Eds. S. Adelman, W.L. Wiese, p. 479
- Rybicki G.B., Hummer D.G., 1994, *A&A* 290, 553
- Schaerer D., 1995, Ph.D. thesis No. 2738, Geneva University, Switzerland
- Schaerer D., 1996, “From Stars to Galaxies: The Impact of Stellar Physics on Galaxy Evolution”, ASP Conf. Series, Vol. 98, Eds. C. Leitherer, U. Fritze - von Alvensleben, J. Huchra, p. 174
- Schaerer D., de Koter A., Schmutz W., Maeder A., 1996a, *A&A* 310, 837 (Paper I)
- Schaerer D., de Koter A., Schmutz W., Maeder A., 1996b, *A&A* 312, 475 (Paper II)
- Schaerer D., Schmutz W., 1992, in: “Atmospheres of Early-type Stars”, Eds. U. Heber, C.S. Jeffery, Lecture Notes in Physics 401, Springer–Verlag, p. 414
- Schaerer D., Schmutz W., 1994a, *A&A* 288, 231
- Schaerer D., Schmutz W., 1994b, *Space Sci. Rev.* 66, 173
- Schaller G., Schaerer D., Meynet G., Maeder A., 1992, *A&AS* 96, 269
- Schmutz W., 1991, in “Stellar Atmospheres: Beyond Classical Models”, Eds. Crivellari, L., Hubeny, I., Hummer, D.G., NATO ASI Series C, Vol. 341, p. 191
- Schmutz W., Hamann W.R., 1986, *A&A* 166, L11
- Sellmaier F., Yamamoto T., Pauldrach A.W.A., Rubin H., 1996, *A&A* 305, L37
- Stasińska G., Schaerer D., 1996, *A&A*, in press
- Snow T.P., Lamers H.J.G.L.M., Lindholm D.M., Odell A.P., 1994, *A&AS* 95, 163
- Vacca W.D., 1994, *ApJ* 421, 140
- Vacca W.D., Garmany C.D., Shull J.M., 1996, *ApJ* 460, 914
- Wessolowski U., Schmutz W., Hamann W.R., 1988, *A&A* 194, 160